Electrochemistry

Received: December 26, 2018
Accepted: January 15, 2019
Published online: March 23, 2019

The Electrochemical Society of Japan

https://doi.org/10.5796/electrochemistry.18-00095

Article

Electrochemistry, **87(3)**, 148–155 (2019)

Prolonged Cycle Life for $Li_4Ti_5O_{12}$//[$Li_3V_2(PO_4)_3$/Multiwalled Carbon Nanotubes] Full Cell Configuration via Electrochemical Preconditioning

Naohisa OKITA,[a] Etsuro IWAMA,[a,b,*] Satoyuki TATSUMI,[a] Trang Nguyên Hồng VÕ,[a] Wako NAOI,[c] McMahon Thomas Homer REID,[b,d,e] and Katsuhiko NAOI[a,b,d,*]

[a] *Department of Applied Chemistry, Tokyo University of Agriculture & Technology, 2-24-16 Naka-cho, Koganei, Tokyo 184-8588, Japan*
[b] *Global Innovation Research Organization, Tokyo University of Agriculture & Technology, 2-24-16 Naka-cho, Koganei, Tokyo 184-8588, Japan*
[c] *Division of Art and Innovative Technologies, K & W Inc., 1-3-16-901 Higashi, Kunitachi, Tokyo 186-0002, Japan*
[d] *Advanced Capacitor Research Center, Tokyo University of Agriculture & Technology, 2-24-16 Naka-cho, Koganei, Tokyo 184-8588, Japan*
[e] *Simpetus LLC., 1 Fitchburg St, Somerville, MA 02143, USA*

* *Corresponding authors: iwama@cc.tuat.ac.jp, k-naoi@cc.tuat.ac.jp*

ABSTRACT

Full cells consisting of nanocrystalline $Li_3V_2(PO_4)_3$ (LVP) positive and standard commercial $Li_4Ti_5O_{12}$ (LTO) negative electrodes demonstrated outstanding cyclability: capacity retention of 77% over 10,000 cycles. We achieved this stable cycle performance by *electrochemical preconditioning* of LTO with Li prior to full-cell cycling. The strategy of Li preconditioning not only allows adjustment of the state of charge (SOC) between negative and positive electrodes, but also gives rise to the formation of a protective covering layer on the LTO surface. As we show, this covering layer plays an important role in preventing a key performance-limiting phenomenon—namely, the deposition of vanadium eluted from LVP onto LTO, which degrades the coulombic efficiency of Li^+ intercalation/deintercalation into LTO crystals—yielding minimal SOC shifts and stable full-cell cycling.

Keywords : Lithium Titanate//Lithium Vanadium Phosphate Full Cells, Electrochemical Preconditioning, State of Charge Shifts, Vanadium Deposition

1. Introduction

Electrical energy storage (EES) devices, in conjunction with technologies such as electric vehicles and renewable power sources, are crucial tools for efficient utilization of electric power in sustainable societies. The central challenge in the design of EES is to maximize energy density and power density while ensuring long lifetimes and safe operation. Perhaps the most famous EES is the lithium-ion battery (LIB); although the current research and development for LIBs are mainly focused on targeting high energy and power densities,[1] their disturbing propensity to ignite or explode poses serious challenges of safety and reliability.[2,3] In contrast, electrochemical capacitors, and specifically *supercapacitors* (SCs), are safe and long-lived devices with high power densities but low energy densities due to limitations on capacity and operating voltage imposed by their charge-storage mechanism, which involves ionic adsorption/desorption on the surface of activated carbon (AC) electrodes. Thus, the challenge of increasing the energy density of SCs is an active topic of current research.[4,5] One promising strategy is the design of *hybrid* supercapacitors, which combine an AC electrode with an electrode made from a high-capacity faradic (pseudocapacitive or battery-like) material such as lithium titanate ($Li_4Ti_5O_{12}$, LTO).[5,6] Efforts to synthesize nanoscale particles of LTO and its composites have dramatically increased the power (C-rate) capability of LTO electrodes, enabling operating speeds comparable to those of AC electrodes (>300 C-rate).[7,8] In particular, in previous work we fabricated nano-LTO//AC hybrid capacitors—which we term *Nanohybrid Capacitors* (NHCs)—which offer the outstanding safety, cycle performance (>10,000 cycles), and power density (6 kW L^{-1} at charge/discharge rates of 300 C or above) of SCs, but with high energy densities on the order of 30 Wh L^{-1}, an 3-fold improvement over SCs.[9,10] Still, the low volumetric energy density of AC positive electrodes (<40 mAh cm^{-3}) continues to limit the volumetric energy density of such hybrid capacitors. This suggests the possibility of dramatically increasing volumetric energy density by replacing the AC positive electrode with an electrode made from battery materials and treated to facilitate ultra-high-speed operation.

Lithium vanadium phosphate (LVP, $Li_3V_2(PO_4)_3$) is a positive-electrode material of polyanion type characterized by strong AO_x bonds (A = B, P, Si); this ensures that there is no release of oxygen from the crystal structure during charge and discharge, and thus minimal risk of ignition.[11] Consequently, LVP offers excellent thermal stability compared to other common positive-electrode materials such as rock-salt $LiCoO_2$ or spinel-form $LiMn_2O_4$. LVP also exhibits high reaction potentials due to inductive effects of phosphoric acid[12] and is thus a promising candidate for positive electrodes.[13] Moreover, lithium ions diffuse in all three dimensions within the solid of LVP, yielding a large value of the Li^+ diffusion coefficient (10^{-9}–10^{-11} cm^2 s^{-1}).[14] This property distinguishes LVP from other phosphate-based polyanionic materials—such as lithium iron phosphate (LFP, $LiFePO_4$), in which the diffusion of lithium ions is constrained to be one-dimensional—and enables device operation at capacitor-grade speeds. One of the challenges associated with the use of LVP cathodes is to circumvent the limitations imposed by the intrinsically low electronic conductivity of LVP (10^{-8}–10^{-9} S cm^{-1}).[15] Strategies such as reducing particle sizes,[16–19] creating carbon-composite materials,[17,18,20] and doping with other metals[19] have been pursued, but have failed to increase charge/discharge speeds above 100 C.

Beyond the challenge of improving power performance, an important issue which has been addressed by only a small number of studies thus far is the performance of full cells using LVP positive

electrodes.[19,21–23] To date, the reported values of volumetric energy density (30–40 Wh L^{-1}) and maximum power density (2–12 kW L^{-1}) for such LVP-based cells have remained limited by the low volumetric density of the negative electrodes, which have involved materials such as AC,[19] hard carbon,[21] and LTO nanowires.[22] A more serious drawback is that the cycle performance of previous devices has been limited to 500–4,000 cycles.[19,21–23] The possibility that this capacity degradation might be caused by the elution of vanadium from LVP was suggested in the patent,[24] but the relationship was left unspecified.

In this study, we design LVP-based full cells that simultaneously achieve high energy, high power density, and long cycle life. First, to realize the full high-power potential of LVP electrodes, we use LVP materials synthesized via our unique technique of *ultracentrifugation* (UC) treatment.[25] UC-treated LVP contains highly crystalline LVP particles, sized 10–100 nm, highly dispersed throughout a matrix of multiwalled carbon nanotubes (MWCNTs).[15] The uc-LVP/MWCNT composites enable high C-rate operation of 96 mAh g^{-1} at 300 C—more than twice the rate possible with AC electrodes—and excellent cycle performance over 10,000 cycles.[15] We assemble full cells consisting of positive electrodes made from the uc-LVP/MWCNT paired with negative electrodes made from standard commercially-available LTO [Section 1]. Then, we successfully identify the mechanism of capacity degradation during full cell cycling and devise a strategy for minimizing its effect on the cycling performance [Sections 1 and 2]. As we show, capacity degradation is caused by gradual shifts of the state of charge (SOC) between two electrodes—namely, an upward SOC shift for uc-LVP/MWCNT and a downward SOC shift for LTO. The SOC shifts are due to a decrease in the coulombic efficiency of the reaction on the LTO side. This, in turn, is due to the deposition of vanadium species on the LTO surface, after elution from LVP particles and diffusion to the negative electrode. Having diagnosed this mechanism for capacity degradation, we propose a cure: *electrochemical preconditioning* of the LTO electrode with Li to minimize SOC shifts. The strategy of *electrochemical preconditioning* not only allows adjustment of SOC, but also gives rise to the formation of a protective covering layer on the LTO surface consisting of electrolyte-decomposition products such as LiF and Li_2CO_3. As we show, this covering layer prevents deposits of vanadium species on the LTO surface and mitigates capacity degradation, resulting in outstanding cycle performance (>10,000 cycles) for the LTO//uc-LVP/MWCNT full-cell configuration.

2. Experimental

2.1 Material

NH_4VO_3 (>99%, Kanto Chemicals), CH_3COOLi (>98.0%, Wako Pure Chemicals), and H_3PO_4 (>85.0%, Wako Pure Chemicals) were used to prepare $Li_3V_2(PO_4)_3$ (LVP). Citric acid (>99.5%, Sigma-Aldrich Corp.) and ethylene glycol (>99.5%, Wako Pure Chemicals) were used as a chelating agent. Multiwalled carbon nanotubes (MWCNTs) with a specific surface area of 240 $m^2 g^{-1}$ [26] were used for the preparation of carbon composite. Ultrapure water (17 MΩ cm) was used as a medium for the entire preparation scheme. $Li_4Ti_5O_{12}$ (LTO, Toho Titanium) was used as a negative electrode in the full cell assembling.

2.2 Preparation of uc-LVP/MWCNT composite under UC treatment

Firstly, three kinds of solution (solution A, B and C) were prepared. Solution A was composed of 0.8000 g of MWCNT and 1.5840 g of H_3PO_4 mixed in 50 ml of ultrapure water. Solution B was composed of 1.0823 g of NH_4VO_3, 0.9251 g of CH_3COOLi and 1.7685 g of citric acid (1.0 eq.) dissolved in 20 ml of ultrapure water. Solution C was composed of 2.2854 g of ethylene glycol dissolved in 10 ml of ultrapure water. Solution A was subjected to the *ultracentrifugation* (UC) treatment[25] at 80°C for 5 min before and after the addition of solution B and C. The uc-treated sol was further dried at 130°C under vacuum for 12 h. The obtained precursor was pre-annealed at 300°C for 3 h in air to remove citric acid and ethylene-glycol-derived amorphous carbon and absorbed water, then left to cool to room temperature (RT). The pre-annealed powder was further annealed at 800°C for 30 min under N_2 flow (RT to 800°C in 3 min, dwell for 30 min, 30 min to cooling to RT) to form the uc-LVP/MWCNT (70/30) composites.

2.3 Physicochemical characterizations of uc-LVP/MWCNT composite

Structure analysis on LVP/MWCNT composite was performed by X-ray diffraction [XRD, MiniFlex (Rigaku), CuKα radiation (λ = 1.54 Å), operating at 40 kV, 15 mA] (see Fig. S1). XRD patterns were recorded in the 10°–60° 2θ range at a scan speed of 0.167° s^{-1}. The carbon content of uc-LVP/MWCNT composite was determined by thermogravimetric analysis under a synthetic air (O_2: 20%, N_2: 80%) using a thermogravimetric/differential thermal analyzer (TG/DTA, Seiko Instruments TG/DTA6300). Surface morphologies on uc-LVP/MWCNT and LTO electrodes before and after charge/discharge were observed by scanning electron microscopy (SEM, Hitachi model S5500) and high-resolution transmission electron microscopy (HRTEM, Hitachi model H9500). X-ray photoelectron spectroscopy (XPS JEOL Ltd. JPS-9200) was carried out using Al X-ray source without Ar etching. Prior to the SEM observation and XPS characterization, the sample electrodes were thoroughly washed by diethyl carbonate (DEC) in the glove box under Ar atmosphere with a dew point <−80°C and then dried for 12 h under vacuum. The quantitative analysis of vanadium in electrolytes and the surface of LTO electrodes was conducted by inductively coupled plasma-mass spectrometry (ICP-MS, Thermo Fisher Scientific, ELEMENT XR) in Toray Research Center. H_2O contents in the electrolytes were measured based on the Karl Fisher method (Mitsubishi Chemical Analytic, CA-6).

2.4 Electrochemical characterization of uc-LVP/MWCNT composite

2032 coin-type Li-metal half-cells were assembled using a negative Li metal electrode and a positive uc-LVP/MWCNT electrode. LTO/LVP Full-cells were assembled using negative LTO and positive uc-LVP/MWCNT electrodes in laminate-type cells. The electrolyte was a mixture of ethylene carbonate and diethyl carbonate (EC:DEC = 1:1) containing 1.0 M of lithium hexafluorophosphate ($LiPF_6$). The separator was a 25 µm-thick monolayer polypropylene separator (Celgard®2400, Celgard). The uc-LVP/MWCNT positive electrodes were prepared by mixing 90 wt.% of the composite and 10 wt.% of polyvinylidene difluoride (PVdF) in n-methyl pyrrolidone (NMP). LTO negative electrodes were prepared by mixing 70 wt.% of the sample, 20 wt.% of acetylene black and 10 wt.% of PVdF in NMP. The mixture was coated on an etched-Al foil (current collector) and dried at 80°C under vacuum for 12 h. Before cell assembling, electrodes were further dried at 120°C for 2 h under vacuum. Using prepared electrodes, cells were assembled in dry room (dew-point temperature <−40°C). Loading masses of LTO and uc-LVP/MWCNT were 1.4 and 1.1 mg cm^{-2} (18 and 20 µm of thickness) on etched Al current collector, respectively, corresponding to the N/P capacity ratio of 1.9. Electrode areas of half-cells and full-cells were 1.54 and 5.0 cm^2, respectively. Charge-discharge tests for the uc-LVP/MWCNT half-cells, LTO half-cells and LTO//(uc-LVP/MWCNT) full-cells were performed in constant-current (CC) charge and discharge modes between 2.5–4.3 V *vs.* Li/Li^+, 1.0–3.0 V *vs.* Li/Li^+ and 1.5–2.8 V, respectively. Current densities for half-cells and full-cells were 10 C-rate for cycling tests and ranged from 1 to

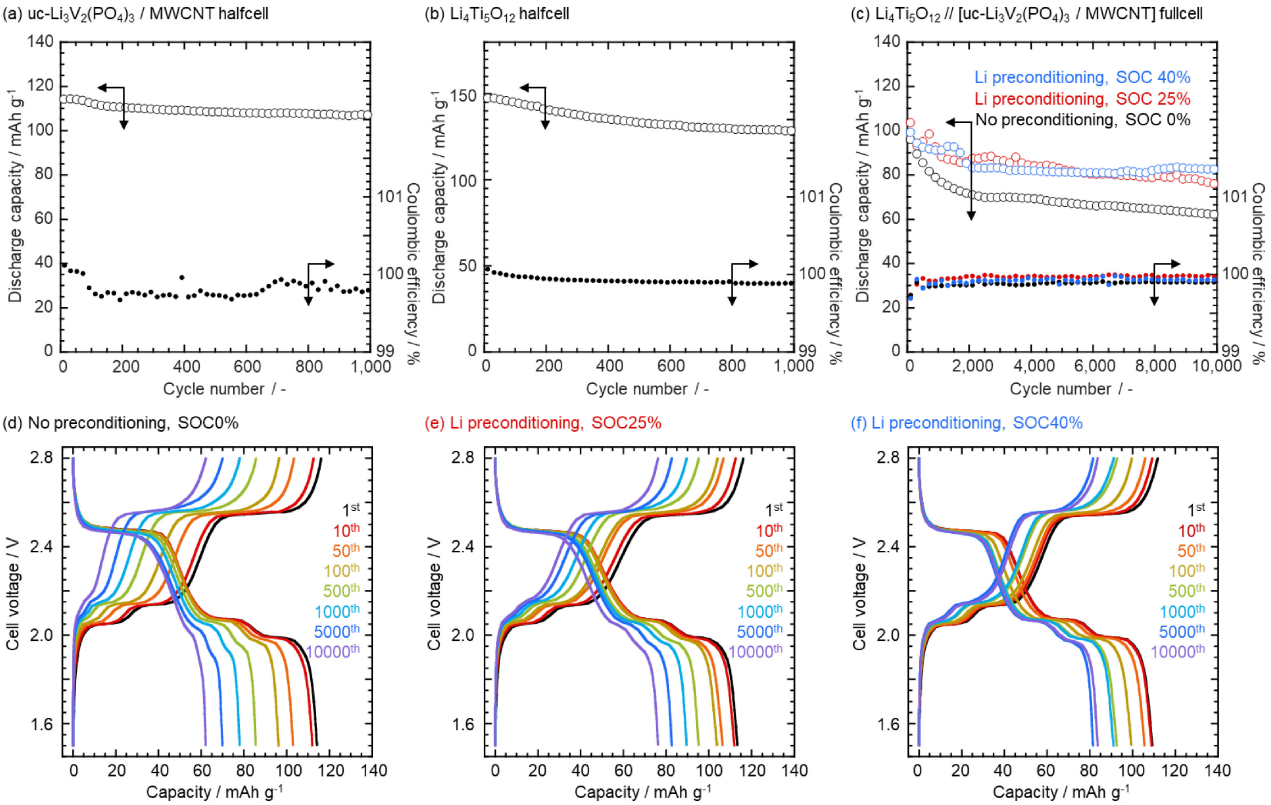

Figure 1. Plots of capacity and coulombic efficiency against cycle of (a) Li//(uc-LVP/MWCNT) and (b) Li//LTO, and (c) LTO//(uc-LVP/MWCNT) full cells with different ratio of Li preconditioning on LTO: SOC 0, 25, and 40%. Charge discharge curves of LTO//(uc-LVP/MWCNT) full cells (d) No preconditioning = SOC 0%, (e) Li preconditioning: SOC 25%, and (f) Li preconditioning: SOC 40%. Note that the capacity in (a) and (b) is per active material and (c) is per LVP, and also the different scales of x-axis in (a), (b), and (c).

480 C-rate in rate tests (see Fig. S2), assuming that 1 C-rate equals 131.5 mA g^{-1}[Li//uc-LVP/MWCNT and LTO//(uc-LVP/MWCNT)] and 175 mA g^{-1}(Li//LTO). Electrochemical preconditioning of LTO was conducted through charge discharge cycling with an additional Li metal electrode in the full cell laminated cells. The details of process are as following: LTO was (i) charged at constant-current constant-voltage (CC-CV) mode with cut-off potential of 1.0 V *vs.* Li/Li^+ and holding time of 1 h, (ii) rested for 24 h, (iii) discharged to 3.0 V at CC mode, (iv) charged and discharged at CC mode between 1.0–3.0 V *vs.* Li/Li^+ for 9 cycles, and then (v) charged at CC mode to the SOC 25 or 40%. At the same time, LVP underwent similar precycling using another additional Li metal in the cell as following: LVP was (i) charged at CC-CV mode with cut-off potential of 4.3 V *vs.* Li/Li^+ and holding time of 1 h, (ii) rested for 24 h, (iii) discharged to 2.5 V at CC mode, and then (iv) charged and discharged at CC mode between 2.5–4.3 V *vs.* Li/Li^+ for 9 cycles. After electrochemical preconditioning process, full cell packages were opened to remove Li metal electrodes, and the re-sealed full cells were cycled thereafter.

3. Results and Discussion

3.1 Cyclability of [LTO//uc-LVP/MWCNT] full cells

As mentioned in the introduction, we have previously reported the LTO//AC hybrid capacitor system—called *Nanohybrid Capacitor* (NHC)[9]—where an AC negative electrode of supercapacitor (SC) was replaced by a nanocrystalline-$Li_4Ti_5O_{12}$/MWCNT composite electrode.[7] The NHC shows the 3-fold energy density of SC, while attaining the high power comparative to SC.[9] To achieve further increase of energy density from NHC, replacement of the AC positive electrode is required by alternatives with higher capacity as well as ultrafast electrochemical characteristics and excellent cycle capability. Here, we assembled the full cells consisting of the uc-LVP/MWCNT (70/30, see Fig. S1) positive and commercially-available LTO negative electrodes. The tested LTO//uc-LVP/MWCNT system exhibits excellent discharge C-rate capability (Fig. S2); 92 mAh g^{-1} at 100 C, and then 55 mAh g^{-1} at 300 C, corresponding to the 76 and 46% of the capacity obtained at 1 C. Besides the Ragone characteristics, another important property for the capacitor application is the long term cyclability. In case of Li metal half cells, LTO and uc-LVP/MWCNT showed excellent cyclability (Figs. 1(a) and 1(b)): the capacity retentions of the initial capacity after 1,000 cycles are 86 and 98% for LTO and uc-LVP/MWCNT, respectively. Both materials show high coulombic efficiency >99.7%, where that for LTO shows slightly higher and stable plots (99.9%). We then simply assembled the LTO//uc-LVP/MWCNT full cells without any pretreatment. In full cell configurations, however, the capacity retention after 1,000 cycles is no more than 68% and continuously decreases to 63% until 2,000 cycles, and then gradually degrades down to 54% after 10,000 cycles as shown in Fig. 1(c). At the 1st cycle, charge discharge curves of the full cell in Fig. 1(d)—tagged as "no preconditioning"—show clear three plateaus at 2.02, 2.10, and 2.51 V in average, corresponding to the typical LVP characteristic of 0.5, 0.5, and 1.0 of Li^+ intercalation/deintercalation per LVP, respectively. With cycling up to 1,000 cycles, one can see the continuous decrease of the first plateau (0.5 Li^+), and this plateau ends up to be almost disappeared. To identify the mechanism responsible for capacity degradation and the disappearance of the first plateau in their charge discharge curves, we disassembled the full cells after 10,000 cycles, and used the cycled negative and positive electrodes to assemble two Li-metal half cells (see Fig. S3). The OCV of the Li//uc-LVP/MWCNT just after reassembling was around 3.65 V *vs.* Li—slightly higher than the 1st plateau of LVP (3.60 V *vs.* Li)[15]—, which is

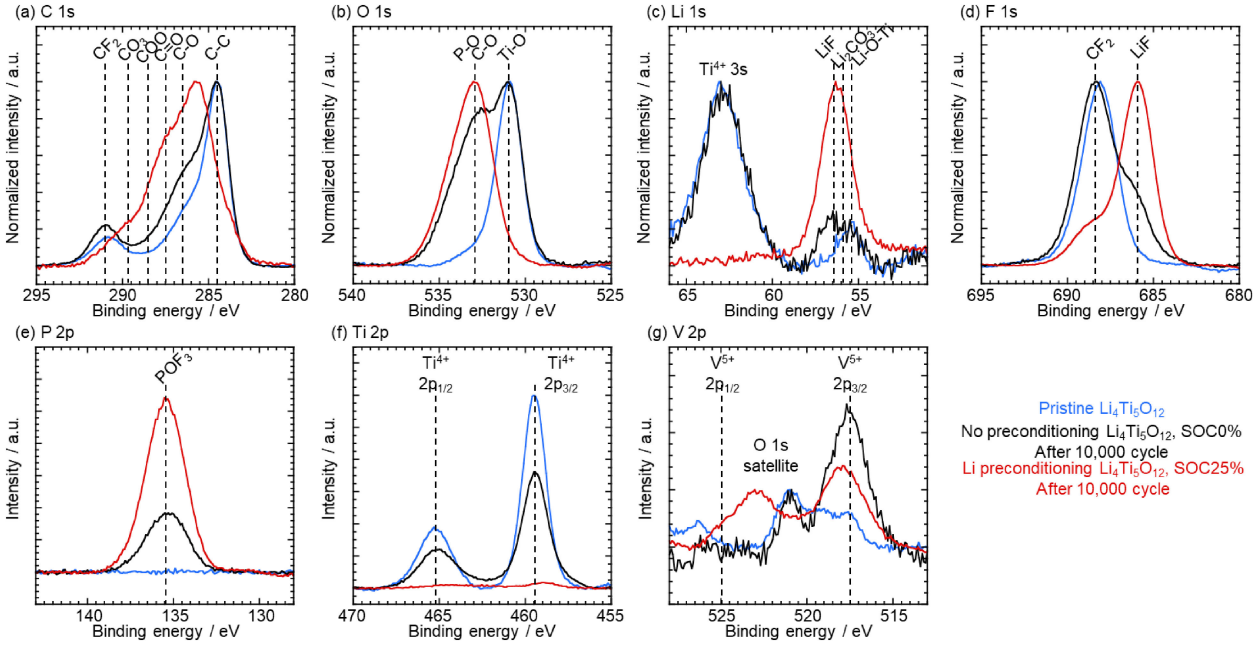

Figure 2. XPS spectra of LTO for the pristine (as prepared), no preconditioning (= SOC 0%) and Li preconditioning (= SOC 25%) after 10,000 cycles in LTO//(LVP/MWCNT) full cell configurations; (a) C1s, (b) O1s, (c) Li1s, (d) F1s, (e) P2p, (f) Ti2p, (g) V2p. Note that the peak intensity of (a)–(d) are normalized at the highest intensity for the better comparison between three samples.

consistent with the disappearance upon cycling of the 1st plateau (Fig. S3(a)). In the direction of discharge, however, the 1st plateau is recovered, and then at 10th cycle, all three plateaus can be observed reversibly as the pristine one. Differently from the uc-LVP/MWCNT, the reassembled Li//LTO half cells exhibited *ca.* 92% in capacity retention of the pristine LTO at the 1st cycle and then 88% at the 10th cycle, only with a small distortion in curve shapes (Fig. S3(b)). All experimental results, both for full cells and reassembled half cells, suggest that there was no significant degradation of electrode materials themselves, and thus that the capacity decrease during the initial 1,000 cycles was due to the appearance of shifts in the state of charge (SOC)[27] between LTO negative and uc-LVP/MWCNT positive electrodes. The high OCV values of the Li//(uc-LVP/MWCNT) half cells are explained convincingly by the hypothesis that uc-LVP/MWCNT shifts to a higher SOC, and that the irreversibility of LTO reaction are responsible for such SOC shift of the positive electrode.[27,28] However, it is contradicted to the coulombic efficiencies obtained for the Li-metal half cells, whereas the LTO cells show higher value (99.9%) than the uc-LVP/MWCNT (99.7%). This contradiction leads to one conclusion that the coulombic efficiency of LTO becomes lower on the condition of the full cell cycling where the uc-LVP/MWCNT was used as a counter electrode of LTO instead of Li metal. Thus, to minimize the effects of such SOC shifts, electrochemical preconditioning process—electrochemical Li predoping on LTO—was conducted using Li//LTO cells, prior to the full cell assembling. The electrochemical preconditioning of LTO negative electrode provides a capacity margin to buffer the effects of SOC shifts regardless of the difference in coulombic efficiency of the reaction.[21] We prepared two types of Li preconditioned LTO with different starting SOC conditions: 25 and 40%. As shown in Fig. 1(c), the full cells using Li preconditioned LTO of 25 and 40% exhibited the high capacity retention even after 10,000 cycles: 66 and 77% of the initial capacity, respectively. Contrary to the no preconditioning sample, the clear 1st plateau can be still observed in their charge discharge curves after 10,000 cycles (see Fig. 1(e) and 1(f)), showing the successful minimization of the SOC shifts of the uc-LVP/MWCNT.

3.2 Elucidation of mechanism of SOC shifts in full cells and the effect of electrochemical preconditioning

As clarified in the section 1, the full cell degradation of LTO//uc-LVP/MWCNT is due to the shift to a high SOC of uc-LVP/MWCNT. However, the question still remains: why the reaction on the LTO negative electrode in full cells became less reversible than that on the uc-LVP/MWCNT positive—which is suggested to be the main reason of the SOC shifts on the positive side—, even though the results on Li-metal half cells suggest that the LTO has slightly, but certainly higher coulombic efficiency compared to the uc-LVP/MWCNT. To elucidate such remaining question, we checked the overall surface composition of LTO with and without electrochemical preconditioning (Li preconditioning) by X-ray photoelectron spectroscopy (XPS), before and after 10,000 cycles in full cell configurations (Fig. 2). Note that the XPS spectra intensity for the four atoms (C1s, O1s, Li1s, and F1s) shown in top of Fig. 2 are normalized for the better comparison between three samples, while the peak intensity for other three atoms (P2p, Ti2p, and V2p) is kept as measured. For the no preconditioning sample after 10,000 cycles, the intensity of Ti2p peaks corresponding to Ti^{4+} $2p_{1/2}$ and $2p_{3/2}$ decreased, compared to the sharp peak for the pristine one. This tendency is in good agreement with obtained results of O1s spectra for the no preconditioning sample, where the P-O/C-O peak intensity became comparative to the Ti-O, indicating that the LTO surface was covered by compounds containing those peaks. The peak corresponding to LiF appeared in Li1s and F1s spectra, while POF_3 (or $Li_xPO_yF_z$) can be also found in P2p spectra. These results suggest that the electrolyte-decomposed products such as $LiPF_6$, EC, and DEC are accumulated on the surface of LTO without Li preconditioning.[29] Another large difference between the pristine and no preconditioning samples is the peaks of V^{5+} $2p_{1/2}$ and $2p_{3/2}$ in the V2p spectra. The detection of such V^{5+} peaks on the LTO surface after 10,000 cycling indicates the elution and subsequent diffusion of vanadium species (V^{n+}) from the uc-LVP/MWCNT positive electrode. Here, to determine the valence state of vanadium species (V^{n+}), whether V^{5+} or its reduced states, is difficult, because of its minute amount (few μg as later shown in Table 1), and the possible redox of V^{4+}/V^{5+} occurs in the potential region close to the LTO reaction (1.55 V

Table 1. Results of ICP-MS on vanadium detection among three LTO samples and corresponding electrolytes: as assembled (soaked in the electrolyte), no preconditioned after 1,000 cycles, and Li preconditioned after 1,000 cycles.

	Vanadium on 5.7 mg of $Li_4Ti_5O_{12}$		Vanadium in 2,000 µL (1.3 g cm^{-3}) of electrolyte		Total amount of vanadium
	ppm	µg	ppm	µg	µg
Soaked $Li_4Ti_5O_{12}$//[uc-$Li_3V_2(PO_4)_3$/MWCNT] fullcell	230	1.3	1.2	3.1	4.4
No preconditioning $Li_4Ti_5O_{12}$//[uc-$Li_3V_2(PO_4)_3$/MWCNT] fullcell, after 1,000 cycles	1400	8.0	0.31	0.81	8.8
Li preconditioning $Li_4Ti_5O_{12}$//[uc-$Li_3V_2(PO_4)_3$/MWCNT] fullcell, SOC 25%, after 1,000 cycles	420	2.4	0.87	2.2	4.6

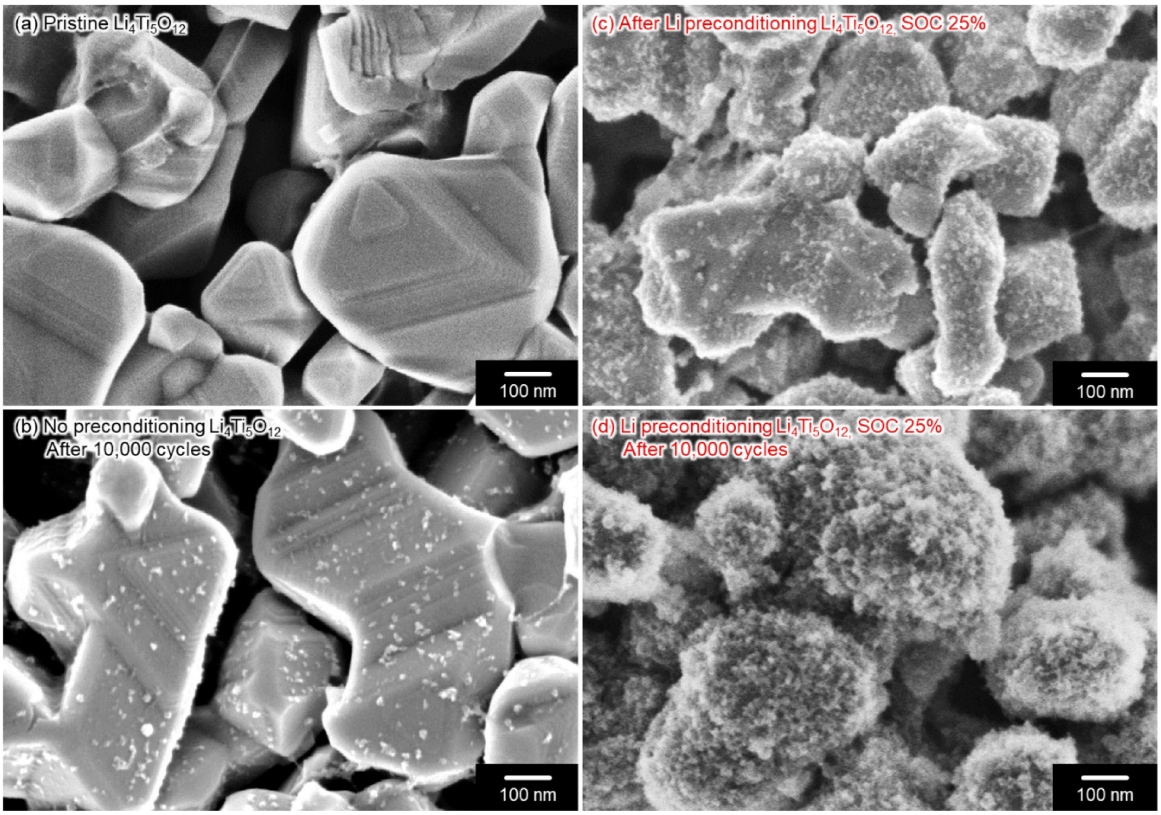

Figure 3. SEM images of LTO electrodes (a) pristine, (b) No preconditioning after 10,000 cycles, (c) Li preconditioning (SOC = 25%) before cycling, and (d) Li preconditioning (SOC = 25%) after 10,000 cycles.

vs. Li/Li$^+$) such as Li_3VO_4.[30] Deposition/accumulation of transition metals such as Mn on the negative electrode in LIBs have been already studied,[31–33] and it is well known that the existence of such transition metal/metal ions on the surface of negative electrodes induces the irreversible decomposition of electrolytes. Thus, it can be expected that the accumulated V^{5+} on the LTO surface catalytically reduces the electrolyte components, leading to the lower coulombic efficiency of LTO side and the subsequent SOC shifts of the uc-LVP/MWCNT. On the Li preconditioned LTO (SOC = 25%), such V^{5+} peaks can be detected but their intensity is much lower compared to the no preconditioning sample. The result well agrees with the quantitative analysis on the amount of vanadium detected from the LTO before and after full cell cycling by inductively coupled plasma-mass spectrometry (ICP-MS). As shown in Table 1, the vanadium amounts detected from the no preconditioning sample after 1,000 cycles is (8.0 µg) the highest compared to other two samples, Li preconditioned LTO after 1,000 cycles (2.4 µg) and the soaked LTO (1.3 µg) which was removed from the full cell after preserved for a week without any cycling. These results indicate that the Li preconditioning of LTO brought about the protective effect from the vanadium accumulation on its surface.

SEM observation on the LTO samples further provides us a clear view of such LTO protection from the vanadium accumulation (Fig. 3). Compared to the smooth surface of the pristine LTO (Fig. 3(a)), small dots ($\phi = ca.$ 10–50 nm)—which may be attributed to mixture of carbonated compounds or LiF—can be clearly seen on the surface of LTO without Li preconditioning after 10,000 cycles (Fig. 3(b)), whose existences were also confirmed in the TEM image (Fig. S4(a)). Furthermore, besides the small dots, very thin film (2–3 nm) can be also observed in the TEM image of the LTO (Fig. S4(b)). Such thin film formed on the LTO surface may be originated from the decomposed organic compounds of electrolytes induced by the deposited vanadium species. Meanwhile, the surface of the Li preconditioned LTO was already covered by the flake-like compounds even before the full cell cycling (Fig. 3(c)), and then the thickness of the surface accumulation was increased with similar morphology after 10,000 cycles (Fig. 3(d)). This coverture on the surface of Li preconditioned LTO well supports the disappearance of

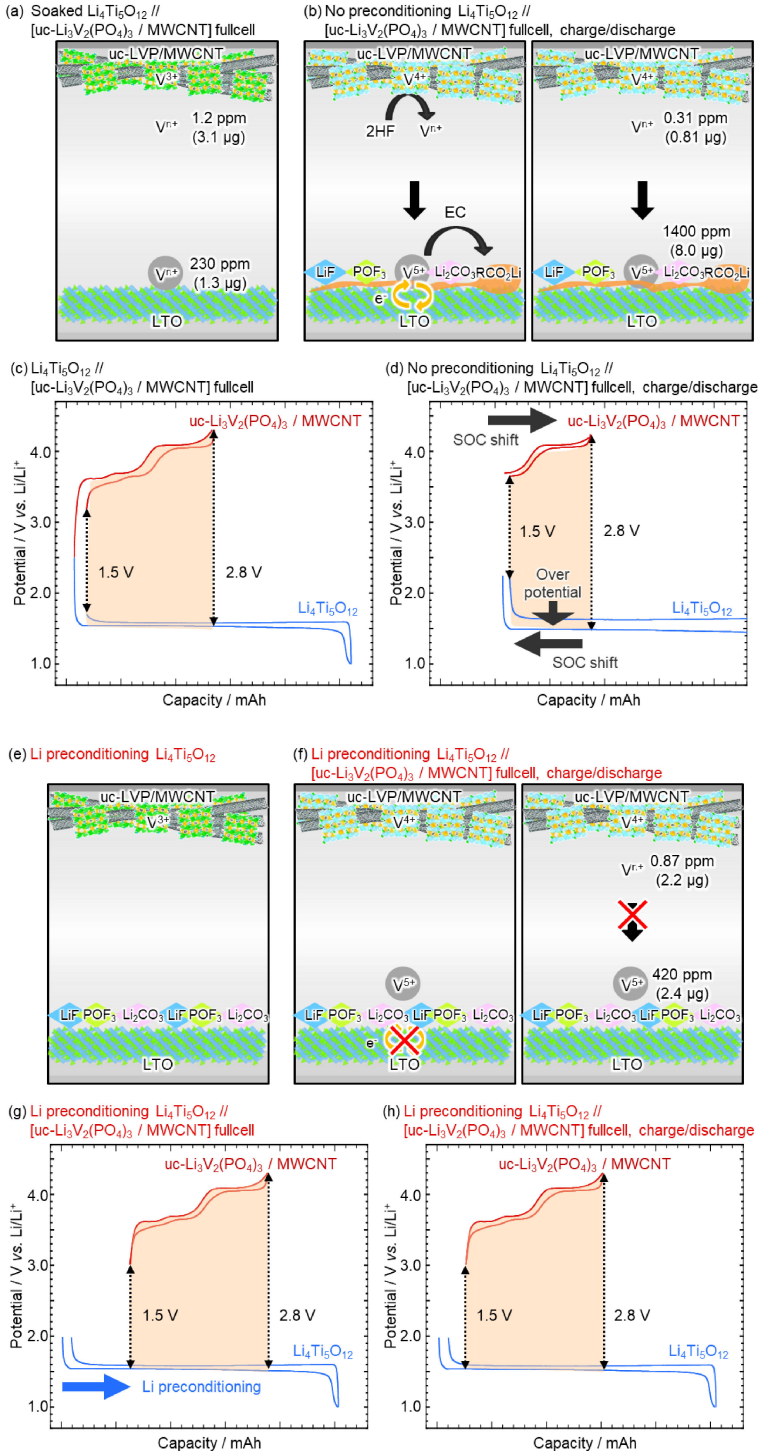

Figure 4. Schematic images of events on the LTO surface during the full cell cycling: (a) just soaked cell (no preconditioning before cycling), (b) no preconditioning during cycling, (e) Li preconditioning before cycling, and (f) Li preconditioning after cycling. Model polarization curves corresponding to LTO negative and uc-LVP/MWCNT positive electrodes in full cell cycling: (c) at initial cycling and (d) after 1,000 cycles for the no preconditioning sample, and (g) at initial cycling and (h) after 1,000 cycles for the Li preconditioning sample.

Ti 2p peaks and significant increase of the peaks attributed to the LiF, carbonates (C-O and C=O), and POF_3. Such coverture on the LTO surface—produced during the Li preconditioning—may play an important role in the protection from the vanadium species deposition during the full cell cycling. Interestingly, these flake-shape compounds on the LTO can be easily removed by ultrasonication of the samples—as observed in Fig. S4(c) and S4(d)—, indicating their weak adhesion on the LTO surface due to the flake morphology (minimum contacts on the surface). Therefore, this minimum-contact coverture is considered to provide the protection of LTO surface without hampering the Li intercalation/deintercalation into LTO.

Combining results of XPS, ICP-MS, and SEM observation, the mechanism of vanadium elution/deposition and the resultant SOC shift of the uc-LVP/MWCNT, as well as its prevention by Li preconditioning of LTO can be drawn as shown in the schematic images of Fig. 4. Even on the condition of soaking of the LTO and uc-LVP/MWCNT in the electrolyte for a week, minute amounts of

vanadium are dissolved from the uc-LVP/MWCNT into the electrolyte as detected 3.1 μg (see Table 1) and also 1.3 μg deposited on the LTO surface. The elution of the vanadium may occur due to the produced HF via hydrolysis of $LiPF_6$[29] in the electrolyte (Fig. 4(a)), where the adsorbed H_2O may be released from the surface of MWCNT and/or LTO. Here, the differences of the measured H_2O contents among the different conditions were within 1–2 ppm or even 0.5 ppm, which are far below the detection limit as 10 ppm (10 μg of H_2O: as the limitation of general Karl Fisher titration apparatus) considering the amount of electrolyte (1 g) used in our laminate-type cells. In the case of the full cell using LTO without Li preconditioning (without any preconditioning of LTO), the vanadium species deposition occurs on the pristine/bare LTO surface, and the deposited vanadium species—which were detected as V^{5+} in XPS spectra—catalytically reacts with the electrolyte, resulted in the formation of thin layer (2–3 nm) and dotted compounds (10–50 nm) on the LTO surface (Fig. 4(b)). Such electrolyte decomposition and further release of H_2O from the LTO surface may induce the production of HF in the electrolyte, which further attacks the LVP particles on the other side and thus provokes further elution of vanadium species.[29] The results of ICP-MS confirmed the increase of vanadium after cycling, as the total amount of dissolved/deposited vanadium (= LTO + electrolyte) doubled from the just soaked sample (4.4 μg) to the no preconditioning sample after 1,000 cycles (8.8 μg). It is considered that, for the no-preconditioning cells, most of vanadium eluted from the LVP was deposited on the LTO surface (8.0 μg). This may be the reason why the amount of vanadium in the electrolyte for the no-preconditioning cells was lower or similar to that for Li preconditioning cells. Such minute amount of vanadium eluted from the uc-LVP does not change its composite morphology (see Fig. S5) nor degrade any electrochemical properties of LVP itself. However, the accumulation of continuous irreversible decomposition on the LTO surface—induced by the deposited vanadium species—gives rise to the difference in the coulombic efficiencies between the LTO and uc-LVP/MWCNT electrodes, and then leads to the gradual SOC shifts as schematically explained in Fig. 4(c) and 4(d). At the initial cycling of the full cell operation, the polarization curves of two electrodes are as originally designed (cell voltage: 1.5–2.8 V) as shown in Fig. 4(c) highlighted in orange. Due to the continuous SOC shifts up to 10,000 cycles, the operation potential range of the uc-LVP/MWCNT shift towards the higher SOC region and thus the LTO goes to the other direction (lower SOC), leading to the capacity degradation with a disappearance of the 1st plateau of LVP (Fig. 4(d)). Furthermore, deposited film and dots on the LTO may inhibit the Li^+ diffusion access from the electrolyte and thus increase overpotential of LTO intercalation, resulted in the slight distortion of LTO polarization and degrades of its exhibited capacity as observed in the reassembled Li//LTO cells (Fig. S3(b)). Applying the preconditioning, LTO is offered to be at higher SOC than no preconditioning sample, which acts as a capacity margin against the SOC shifts regardless of the difference in coulombic efficiency between positive and negative electrodes. Moreover, the surface of the Li preconditioned LTO is covered by flake-shape compounds containing LiF, and Li_2CO_3, which minimize the deposition of vanadium species on the LTO surface (2.4 μg) as shown in Fig. 4(e) and 4(f). Such LTO surface protection may prevent the subsequent events leading to the vanadium elution from the positive electrode (Fig. 4(f)), as confirmed by ICP-MS where the total vanadium amount (4.6 μg) remained almost the same as the soaked sample (4.4 μg). Combination of these two factors—capacity margin against SOC shifts and surface protection of LTO—assured stable charge discharge behavior in the full cell cycling (Fig. 4(g) and 4(h)), and brought about the excellent cycle performance: 77% of the initial capacity retention over 10,000 cycles.

4. Conclusions

In conclusion, we successfully assembled full cell system based on the uc-LVP/MWCNT positive paired with a commercially-available LTO negative electrode and the outstanding long cycle life configuration—over 10,000 with 77% capacity retention of its initial capacity—was demonstrated for the full cell cycling. Such stable cycle performance was achieved thanks to the electrochemical preconditioning (= Li preconditioning of LTO, SOC = 25 and 40%) conducted prior to the full cell assembling, while the capacity retention without preconditioning falls to 54%. In the process of elucidation of the Li-preconditioning effects on cycle performances, it was found that minimization of the vanadium elution from the LVP and the subsequent deposition on the LTO surface play an important role for the stable cycling. Combined results of XPS, ICP-MS and SEM observation suggest that the deposited vanadium species on the LTO surface induces the decomposition of electrolytes and production of HF. The irreversible electrolyte decomposition leads to a decrease in the coulombic efficiency of Li^+ intercalation/deintercalation into LTO crystals, resulted in the gradual shift between two electrodes: higher SOC for uc-LVP/MWCNT positive and lower SOC for LTO negative electrodes. Additionally, the produced HF is considered to induce further elution of vanadium from the uc-LVP/MWCNT, accelerating the SOC shifts and degradation in the full cell capacity. Li preconditioning of LTO was found to be effective as a countermeasure, because of the given capacity margin to minimize the effect of SOC shifts, and the formation of the protective coverture on the LTO surface—composed of such as LiF and Li_2CO_3—from the undesirable vanadium deposition.

Supporting Information

The Supporting Information is available on the website at DOI: https://doi.org/10.5796/electrochemistry.18-00095.

Acknowledgments

This study was supported by the Global Innovation Research Organization in TUAT. This study was supported by JSPS Grant-in-Aid for Scientific Research (KAKENHI) A under Grant No. JP25249140, KAKENHI C under Grant No. JP17K05962, KAKENHI Grand-in-Aid for Young Scientists B under Grant No. JP16K17970, and the Center of Innovation Program from Japan Science and Technology Agency (A-STEP; AS282S002d).

References

1. J. B. Goodenough and Y. Kim, *Chem. Mater.*, **22**, 587 (2010).
2. N. Williard, W. He, C. Hendricks, and M. Pecht, *Energies*, **6**, 4682 (2013).
3. J. M. Loveridge, G. Remy, N. Kourra, R. Genieser, A. Barai, J. M. Lain, Y. Guo, M. Amor-Segan, A. M. Williams, T. Amietszajew, M. Ellis, R. Bhagat, and D. Greenwood, *Batteries*, **4** (2018).
4. M. Salanne, B. Rotenberg, K. Naoi, K. Kaneko, P. L. Taberna, C. P. Grey, B. Dunn, and P. Simon, *Nat. Energy*, **1**, 16070 (2016).
5. Z. Lin, E. Goikolea, A. Balducci, K. Naoi, P. L. Taberna, M. Salanne, G. Yushin, and P. Simon, *Mater. Today* (2018).
6. G. G. Amatucci, F. Badway, A. Du Pasquier, and T. Zheng, *J. Electrochem. Soc.*, **148**, A930 (2001).
7. K. Naoi, S. Ishimoto, Y. Isobe, and S. Aoyagi, *J. Power Sources*, **195**, 6250 (2010).
8. E. Zhao, C. Qin, H.-R. Jung, G. Berdichevsky, A. Nese, S. Marder, and G. Yushin, *ACS Nano*, **10**, 3977 (2016).
9. K. Naoi, W. Naoi, S. Aoyagi, J.-i. Miyamoto, and T. Kamino, *Acc. Chem. Res.*, **46**, 1075 (2013).
10. K. Naoi, S. Ishimoto, J.-i. Miyamoto, and W. Naoi, *Energy Environ. Sci.*, **5**, 9363 (2012).
11. C. Masquelier and L. Croguennec, *Chem. Rev.*, **113**, 6552 (2013).
12. A. Yamada, S. C. Chung, and K. Hinokuma, *J. Electrochem. Soc.*, **148**, A224 (2001).

13. S. C. Yin, H. Grondey, P. Strobel, M. Anne, and L. F. Nazar, *J. Am. Chem. Soc.*, **125**, 10402 (2003).
14. X. H. Rui, N. Ding, J. Liu, C. Li, and C. H. Chen, *Electrochim. Acta*, **55**, 2384 (2010).
15. K. Naoi, K. Kisu, E. Iwama, Y. Sato, M. Shinoda, N. Okita, and W. Naoi, *J. Electrochem. Soc.*, **162**, A827 (2015).
16. L. Zhang, H. Xiang, Z. Li, and H. Wang, *J. Power Sources*, **203**, 121 (2012).
17. X. Rui, D. Sim, K. Wong, J. Zhu, W. Liu, C. Xu, H. Tan, N. Xiao, H. H. Hng, T. M. Lim, and Q. Yan, *J. Power Sources*, **214**, 171 (2012).
18. X. Zhang, R.-S. Kühnel, H. Hu, D. Eder, and A. Balducci, *Nano Energy*, **12**, 207 (2015).
19. M. Secchiaroli, G. Giuli, B. Fuchs, R. Marassi, M. Wohlfahrt-Mehrens, and S. Dsoke, *J. Mater. Chem. A*, **3**, 11807 (2015).
20. C. Wang, W. Shen, and H. Liu, *New J. Chem.*, **38**, 430 (2014).
21. Y. Liu, B. Yang, X. Dong, Y. Wang, and Y. Xia, *Angew. Chem., Int. Ed.*, **56**, 16606 (2017).
22. C. Liu, S. Wang, C. Zhang, H. Fu, X. Nan, Y. Yang, and G. Cao, *Energy Storage Mat.*, **5**, 93 (2016).
23. W.-f. Mao, N.-n. Zhang, Z.-y. Tang, Y.-q. Feng, and C.-x. Ma, *J. Alloys Compd.*, **588**, 25 (2014).
24. K. Baba, Y. Kiy, S. Kudo, T. Sakuraba, inventors, Subaru Corp, Nippon Chemical Industrial Co Ltd and Assignee, Patent, WO2014002584A1 (2013).
25. E. Iwama, P. Simon, and K. Naoi, *Curr. Opin. Electrochem.*, **6**, 120 (2017).
26. E. Iwama, N. Kawabata, N. Nishio, K. Kisu, J. Miyamoto, W. Naoi, P. Rozier, P. Simon, and K. Naoi, *ACS Nano*, **10**, 5398 (2016).
27. Y. Kobayashi, T. Kobayashi, K. Shono, Y. Ohno, Y. Mita, and H. Miyashiro, *J. Electrochem. Soc.*, **160**, A1181 (2013).
28. B. Aktekin, M. J. Lacey, T. Nordh, R. Younesi, C. Tengstedt, W. Zipprich, D. Brandell, and K. Edström, *J. Phys. Chem. C*, **122**, 11234 (2018).
29. J. Wang, Z. Liu, G. Yan, H. Li, W. Peng, X. Li, L. Song, and K. Shih, *J. Power Sources*, **329**, 553 (2016).
30. P. Rozier, E. Iwama, N. Nishio, K. Baba, K. Matsumura, K. Kisu, J. Miyamoto, W. Naoi, Y. Orikasa, P. Simon, and K. Naoi, *Chem. Mater.*, **30**, 4926 (2018).
31. M. Evertz, F. Horsthemke, J. Kasnatscheew, M. Börner, M. Winter, and S. Nowak, *J. Power Sources*, **329**, 364 (2016).
32. C. Zhan, T. Wu, J. Lu, and K. Amine, *Energy Environ. Sci.*, **11**, 243 (2018).
33. J. Wandt, A. Freiberg, R. Thomas, Y. Gorlin, A. Siebel, R. Jung, H. A. Gasteiger, and M. Tromp, *J. Mater. Chem. A*, **4**, 18300 (2016).